

## PAPER



Cite this: *J. Mater. Chem. B*, 2017,  
5, 7819

## Synthesis, coating, and drug-release of hydroxyapatite nanoparticles loaded with antibiotics†

Ori Geuli,<sup>a</sup> Noah Metoki,<sup>b</sup> Tal Zada,<sup>a</sup> Meital Reches,<sup>ib</sup>\*<sup>a</sup> Noam Eliaz,<sup>ib</sup>\*<sup>b</sup> and Daniel Mandler,<sup>ib</sup>\*<sup>a</sup>

Post-surgery infections are considered the most challenging complication in the orthopedic and dental field. The local release of antibiotics is evidently highly efficient in delivering the drug to the vicinity of the infected area without the risk of systemic toxicity. Bioactive materials, such as hydroxyapatite (HAp) among other calcium phosphates, are reputed as superior antibiotic vehicles, and combine drug-delivery properties and enhanced osteoconductivity. Here, we report on the single-step electrophoretic deposition (EPD) of drug-loaded HAp nanoparticles (NPs) on titanium implants. This approach provides a purely bioactive coating with drug delivery properties in a simple, economic, and fast process. We synthesized pure HAp NPs with 12.5% and 12.8% loading weight percentages of gentamicin sulfate (Gs) and ciprofloxacin (Cip), and electrophoretically deposited them on a titanium substrate. Furthermore, we co-deposited Gs-HAp and Cip-HAp in one-step to yield a drug-loaded system consisting of two types of antibiotics. The drug-loaded NPs as well as the coatings were carefully characterized. The release profiles of the Gs-HAp and Cip-HAp NP coatings showed prolonged release of up to 10 and 25 days, respectively. The bioactivity test revealed superior bioactivity with enhanced precipitation of HAp crystals along with inorganic minerals, such as Mg<sup>2+</sup>, Na<sup>+</sup>, and Cl<sup>-</sup>. The antibacterial *in vitro* tests of the Cip and Gs-HAp coatings showed efficient inhibition of *Pseudomonas aeruginosa* bacteria.

Received 6th August 2017,  
Accepted 6th September 2017

DOI: 10.1039/c7tb02105d

rsc.li/materials-b

### 1. Introduction

The prophylaxis of infection and its consequences remain a considerable challenge in orthopedic and dental implantation. Post-surgery osteomyelitis is the main reason limiting the success of implantation, which usually results in implant removal. Osteomyelitis, an infectious inflammation of the bone, is primarily caused by three different bacteria species: *Staphylococcus*, *Enterobacteriaceae*, and *Pseudomonas*, where the Gram-positive *S. aureus* (~2/3 of chronic osteomyelitis cases) and *S. epidermis* are the most common pathogens.<sup>1–3</sup> Aminoglycosides, such as gentamicin (Gs), have a wide antibacterial spectrum against both Gram-positive and Gram-negative bacteria. Therefore, aminoglycosides are usually selected as an efficient antibacterial agent in osteomyelitis treatment.<sup>1</sup> On the other hand, fluoroquinolones, such as ciprofloxacin

(Cip), have gained much attention due to their low minimal inhibitory concentration (0.25–2 µg mL<sup>-1</sup>) for most of the bacteria related to osteomyelitis.<sup>4,5</sup>

In general, implant-related infections are based on bacterial adhesion, and in severe cases biofilm formation, at the implantation site. The inhibition of bacterial adhesion is considered the most crucial step in preventing implant-related infections.<sup>6</sup> The conventional treatment of osteomyelitis is primarily based on systemic antibiotic therapy and debridement of the infected tissues.<sup>2,7,8</sup> Conventional systemic delivery of antibiotics (intravenously or orally) may cause systemic toxicity with associated renal and liver complications due to inefficient penetration into the cells and high concentrations of antibiotic intake.<sup>6,9</sup> Therefore, local release of antibiotics has become more popular over the traditional antibiotic administration.

Treatment of osteomyelitis with local delivery of antimicrobial agents is a novel therapeutic approach, which provides elevated antibiotic concentrations at the site of infection without the risk of systemic toxicity. Local antibiotic release is achieved by introducing antibiotics into a matrix, which can be classified into two types: biodegradable and non-biodegradable. A non-biodegradable matrix, such as polymethylmethacrylate (PMMA) beads, has been commercially approved by the US FDA.<sup>10,11</sup>

<sup>a</sup> Institute of Chemistry, The Hebrew University of Jerusalem, Jerusalem 9190401, Israel. E-mail: daniel.mandler@mail.huji.ac.il, meital.reches@mail.huji.ac.il

<sup>b</sup> Biomaterials and Corrosion Lab, Department of Materials Science and Engineering, Tel-Aviv University, Ramat Aviv 6997801, Israel. E-mail: neliaz@tau.ac.il

† Electronic supplementary information (ESI) available. See DOI: 10.1039/c7tb02105d

Although PMMA carriers have been proven to treat osteomyelitis efficiently, their major limitation is a required subsequent surgery for beads removal. At the same time, biodegradable materials have been extensively investigated for the local release of antibiotics.<sup>12</sup> Poly(lactic acid) (PLA), poly(caprolactone) (PCL),<sup>12</sup> poly(lactide-co-glycolide) (PLGA),<sup>13</sup> and chitosan<sup>14</sup> have been used as vehicles for antibiotics delivery. Although these biodegradable systems possess excellent biocompatibility and do not require post-surgery implant removal due to complete resorption, their tendency to enhance bone regeneration is very limited.<sup>15</sup>

The utilization of drug-loaded calcium phosphate-based coatings, such as hydroxyapatite (HAp), and bioglass provides additional value, such as osteoconductivity along with antibacterial properties. HAp,  $(\text{Ca}_5(\text{PO}_4)_3\text{OH})$ , coatings have been massively studied due to their excellent biocompatibility, non-toxicity, non-immunogenicity, and superior bioactivity in promoting bone regeneration.<sup>16–20</sup> In addition, HAp has fundamental adsorption capacity due to its positively charged surface ( $\text{Ca}^{2+}$ ) attracting anion pairing interactions with deprotonated carboxyl groups ( $-\text{CO}_2^-$ ), and negatively charged groups,  $\text{PO}_4^{3-}$ , which promote interactions with protonated amines ( $-\text{NH}_3^+$ ).<sup>21</sup> Therefore, combining HAp coatings with antibiotics is considered a very promising approach, which may guarantee bone-implant integration without bacterial adhesion. Currently, plasma spray coating of HAp is the most popular FDA approved method for medical use.<sup>22,23</sup> This method is carried out at high temperature, and therefore incorporating organic materials in the process is impossible. Alternative coating techniques, such as dip coating,<sup>24</sup> electrochemical deposition,<sup>25</sup> electrospray deposition,<sup>26</sup> and electrophoretic deposition (EPD),<sup>27</sup> seem to

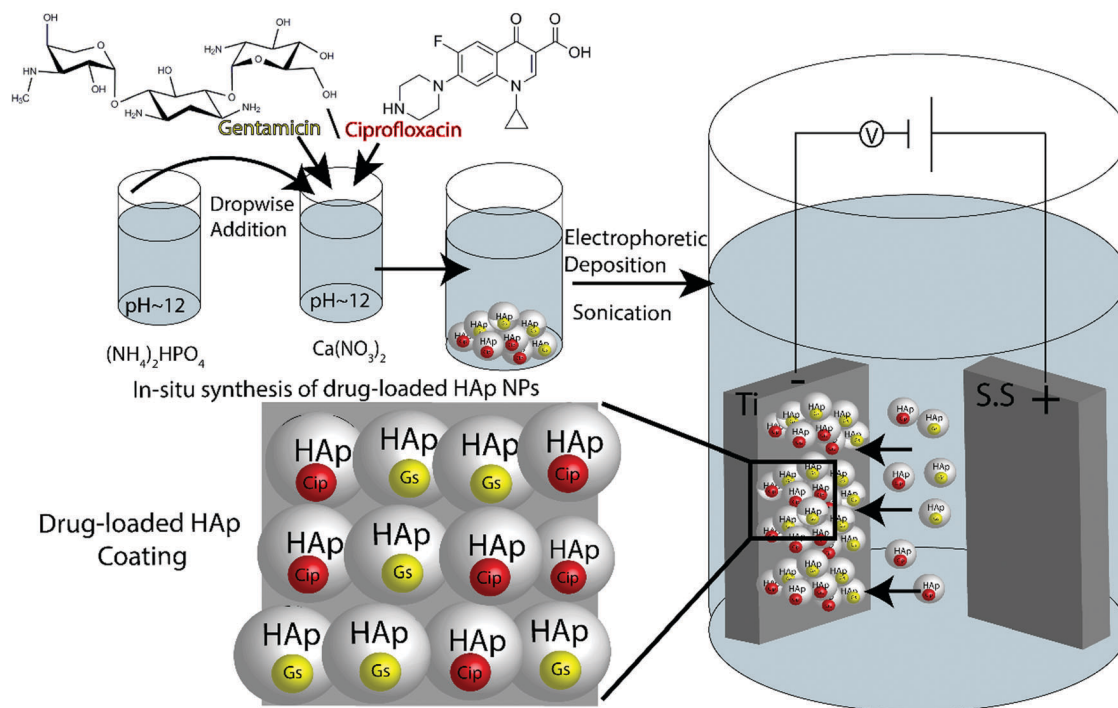
be more compatible for antibiotic incorporation. For example, Tian *et al.* reported the successful incorporation of Gs after immersing an  $\text{Fe}_3\text{O}_4$ /carbonated HAp coating in a Gs solution.<sup>28</sup> Laurent and coworkers used a commercial HAp/tricalcium phosphate bone substitute for Gs loading by immersion.<sup>29</sup> Pishbin *et al.* reported on the co-EPD of Gs with a bioactive glass/chitosan nanocomposite coating. They showed release of antibiotics for a prolonged time of up to 8 weeks as well as good cellular attachment.<sup>30</sup> Zheng and coworkers deposited electrochemically a composite made of calcium phosphate/chitosan and carbon nanotubes for increasing the Gs loading by immersion.<sup>31</sup>

Previously, we reported on a novel technique to coat titanium implants by electrochemically driven deposition of HAp NPs.<sup>25</sup> Here, we present a new approach for a single-stage deposition of pre-loaded HAp NPs with antibiotics onto a titanium implant (Scheme 1). Our method is based on loading pure HAp NPs with Gs or Cip, followed by their EPD to produce an osteoconductive and antibacterial coating that releases more than 80% of Cip and 30% of Gs within 25 days. Moreover, we succeeded in co-depositing simultaneously both Gs-HAp and Cip-HAp NPs to produce a drug-loaded coating that contained two antibiotics.

## 2. Materials and methods

### 2.1 Drug-loaded HAp NP synthesis

4.722 g of  $\text{Ca}(\text{NO}_3)_2$  (ACS EMSURE<sup>®</sup>, Merck) was dissolved in 18 mL of deionized water (Barnstead, Dubuque) using a magnetic stirrer. The pH of the solution was adjusted to 12 by adding 0.6 mL



Scheme 1 Schematic illustration of the synthesis and deposition of antibiotic-loaded HAp NPs.

of ammonium hydroxide (25%, Baker Analyzed<sup>®</sup>, J. T. Baker) and 17.4 mL of water. For Gs-HAp NPs, 10 mg mL<sup>-1</sup> of Gs (Bio-Reagent, Sigma-Aldrich) was added. For the Cip-loaded HAp NPs, 10 mg mL<sup>-1</sup> of Cip (>98%, BDL) was added. 6.6 mL of ammonium hydroxide was added in order to enhance the Cip dissolution. 1.584 g of (NH<sub>4</sub>)<sub>2</sub>HPO<sub>4</sub> (BioUltra ≥99.0%, Sigma) was dissolved in 30 mL of water while stirring. The pH of the solution was adjusted to 12 by adding 15 mL of concentrated ammonium hydroxide and another 19 mL of deionized water. The Ca/P molar ratio in all the solutions was 1.667. The diammonium phosphate solution was slowly added dropwise using a separatory funnel to the calcium nitrate solution while vigorously stirring. The slow addition resulted in a turbid suspension. The latter was boiled for 1 h. Then, the suspension was cooled to room temperature and left until the pH decreased to 7 (after *ca.* 3 days) as a result of ammonia evaporation. Boiling for 1 h should not damage the antibacterial activity of the antibiotics due to their high thermal stability.<sup>32</sup> The precipitated NPs were washed with water and centrifuged at 10000 rpm for 5 min. The HAp NPs loaded with antibiotics precipitated and were collected and freeze-dried. The loaded HAp NPs were characterized by X-ray diffraction (XRD, Bruker, D9 Advance), X-ray photoelectron spectroscopy (XPS, Axis Ultra), high-resolution scanning electron microscopy (XHR-SEM, FEI Magellan<sup>™</sup> 400L) combined with energy-dispersive X-ray spectroscopy (EDS), and high-resolution transmission scanning electron microscopy (HR-TEM, Tecnai F20 G2). All the XRD results were compared to the ICSD (Inorganic Crystal Structure Data) files.

## 2.2 Drug-loaded HAp NP suspension preparation

A Gs-HAp NP dispersion was prepared by adding 0.5% (w/w) NPs to various organic solvents: ethanol, 2-propanol, and *n*-butanol (all BEAKER ANALYZED<sup>®</sup> Reagent). Triethanolamine (TEOA, BEAKER ANALYZED<sup>®</sup> Reagent) was added as a dispersing agent (4 mL L<sup>-1</sup>) to the alcohols to increase the suspension stability. A Cip-HAp NP dispersion was prepared by adding 0.25% (w/w) NPs to 2-propanol. A combined dispersion of Gs-HAp and Cip-HAp was prepared by adding 0.25% w/w of each of the NPs to 2-propanol followed by the addition of TEOA (2 mL L<sup>-1</sup>). Stable nanoparticle dispersions were obtained following sonication of 20 mL of solution for 20 min at 90% amplitude, with a pulse rate of 1 s on, 1 s off, using a tip-sonicator (Sonics, Vibra cell). The suspension stability was examined by measuring the (zeta) ζ-potential and particle distribution size (Zetasizer, Malvern ZS).

## 2.3 Titanium surface pretreatment

Ti (Grade 4) plates and Ti-6Al-4V rods were purchased from Barmil Ltd. The surface area of the Ti plate was 1.08 cm<sup>2</sup>, and that of the Ti-6Al-4V rod was 2.68 cm<sup>2</sup>. The Ti plates were manually ground on Grit 600 grinding paper (Microcut<sup>®</sup>, Buehler), rinsed in acetone, ethanol and water in an ultrasonic bath (Elmasonic P, Elma) for 10 min, and etched in (30%)HF/(65%)HNO<sub>3</sub> (2 vol% and 20 vol%, respectively) for 1.5 min. Commercial dental implants made of Ti-6Al-4V from SGS Dental Implants (Schaan, Liechtenstein) were tested.

## 2.4 Drug loading determination

The amount of drug loaded into the HAp NPs was determined by a quantitative spectrophotometric method. Cip has maximum absorption at 271 nm. A calibration curve was prepared by measuring the absorbance at 271 nm of standard solutions of Cip (2–20 μg mL<sup>-1</sup>) using a UV-Vis spectrophotometer (Evolution 201, Thermo Fisher Scientific).<sup>5,33</sup> Gs has poor UV-Vis absorption, and therefore an indirect spectrophotometric method<sup>34</sup> was required, using fluorescamine (≥98%, Sigma) as a derivatizing agent.<sup>35</sup> The maximum absorbance of the chromophoric product was determined at 391 nm. A calibration curve was formed by measuring the absorbance of a series of Gs solutions (0–80 μg mL<sup>-1</sup>) with a constant amount of fluorescamine. The detection limit (DL) was calculated based on the calibration graph according to ICH.<sup>36</sup> Determination of the amount of either Gs or Cip in the HAp NPs was accomplished by dissolving 10 mg of the drug-loaded HAp NPs in 5 mL HCl (0.5 M) followed by neutralization by 5 mL NaOH (0.5 M) and dilution with 40 mL of water. The absorbance of 5 mL of the sample was measured according to the maximum absorbance of the relevant drug, and the concentration was calculated based on the calibration curve. The loading percentage was evaluated by dividing the total drug amount in the solution by the weight of the drug-loaded NPs.

## 2.5 Electrophoretic deposition

Coating of the various samples was achieved by EPD (Major Science, Mini 300) in a conventional two-electrode cell. Pretreated Ti (Grade 4) or Ti-6Al-4V was used as an anode, whereas stainless steel 316L with the same dimensions was the cathode. The two electrodes were placed parallel, the distance between them being approximately 5 mm. For each experiment, a fresh 20 mL dispersion (0.5% w/w Gs-HAp and 0.25% w/w Cip-HAp) was used. A constant potential of 80 V for Gs-HAp and 40 V for Cip-HAp were applied for 5 min. For co-deposition of Gs-HAp (0.25% w/w) and Cip-HAp (0.25% w/w), a potential of 60 V was applied for 5 min. After deposition, the samples were left to dry under ambient conditions. The commercial dental implants were used also as substrates. The weight gain was determined by weighing the substrate before and after drying. The total amount of drug in the coating was calculated based on the loading percent of the drug in the NPs. The coated Ti substrates were weighed before and after deposition using a microanalytical balance (Mettler Toledo, XP26).

## 2.6 Coating characterization

The coated substrates were analyzed by XRD ( $2\theta = 10\text{--}60^\circ$  at a step size of 0.02 deg s<sup>-1</sup>). High-magnification images of the coated surfaces were acquired by XHR-SEM and environmental SEM (ESEM, FEI Quanta 200FEG). The thickness of the samples was measured by a profilometer (P15, KLA-Tencor). Element analysis was performed by EDS and XPS. Fourier transform infrared (FTIR) spectra were recorded using a Bruker Vertex 70V. A deuterated triglycine sulfate (DTGS) detector was used for the wavenumber spectra. The samples were scanned 128 times at 4 cm<sup>-1</sup> resolution. The spectra were recorded

between 500 and 5000  $\text{cm}^{-1}$ . The strength of adhesion of the Cip-HAP and Gs-HAP coatings to the metal substrate was tested by a standard tension test.<sup>37</sup> Each test specimen was an assembly of a coated sample and a matching uncoated sample with exactly the same dimensions and surface pretreatment, which included grit blasting by alumina powder (high purity white alumina powder from Calbex Mineral Trading, Inc). The blasting machine was model SandyPlus GD from Carlo DeGiordi. The blasting parameters were: a grit size of F200–F180 (59–68  $\mu\text{m}$ ), a pressure of approximately 6 atm, and a working distance of 3 cm or higher. The grit blast operation lasted until a dark grey shade evenly covered the sample. The sample was then washed with DI water and cleaned ultrasonically in acetone. The two parts of the assembly were bonded together by a thin layer of a DP-420 Off-White 3M™ Scotch-Weld™ Epoxy Adhesive, which was left to cure at room temperature for 24 h while exposing each assembly to a compression stress of 138 kPa (20 psi). The sample was held by the grips of an MTS 20/M tensile machine. The tensile load was applied at a constant cross-head velocity of 0.5  $\text{mm min}^{-1}$ . This velocity, which is slightly lower than that recommended in ref. 38, was found to be most suitable for the samples used in this study, where both the cross-section and the thickness of the coating were smaller than the values referred to in ref. 38. Three assemblies were tensile tested. In addition to monitoring the maximum applied load, the locus of failure was determined by inspecting both parts of the assembly by means of ESEM-EDS. The calculation of the drug wt% was conducted by microanalysis (Perkin-Elmer 2400 series II analyzer).

### 2.7 Drug release studies

The coated titanium substrates were immersed in phosphate-buffered saline (PBS, pH 7.4, Sigma) at  $37 \pm 1$  °C in a humidity chamber (Memmert, HCP 108) for 25 days. Every 5 days the solution was replaced by a fresh PBS solution, and the former was spectrophotometrically analyzed. For each drug-loaded HAP coating, the experiment was conducted in triplicate.

### 2.8 Bioactivity test

Simulated body fluid (SBF) was prepared according to a previous procedure.<sup>39,40</sup> The coated implant was soaked in SBF solution at 37 °C for 4 weeks in a thermostatic bath (Firstek, B300). Every 5 days the SBF solution was replaced by a fresh one. The morphology of the implant was examined by ESEM and XHR-SEM.

### 2.9 Antibacterial activity

Gs-HAP and Cip-HAP coatings were scraped from the titanium substrates after EPD. The scraped coatings were introduced into PBS solution and sonicated for 1 h in order to release the antibiotics. Afterwards, the solutions were centrifuged for 10 min at 5000 rpm. The supernatants (20  $\mu\text{L}$ ) were dropped into agar plates, which contained *Pseudomonas aeruginosa* bacteria. The agar plates were incubated for 6 h at 37 °C. After incubation, the inhibition zones were photographed and measured by a ruler. Each experiment was conducted three times. Pure Gs and Cip solutions (100  $\mu\text{g mL}^{-1}$  in PBS) were used as a

positive control, and supernatants from scraped pristine HAP coatings were used as a negative control.

## 3. Results and discussion

### 3.1 Preparation and characterization of drug-loaded HAP NPs

Drug-loaded HAP NPs were synthesized based on the precipitation reaction between calcium and phosphate ions under basic conditions,<sup>41,42</sup> where the antibiotics were introduced into the calcium solution prior to its dropwise addition to the phosphate solution. The interaction between the calcium ions and Gs has been reported in various systems.<sup>43–45</sup> At the same time, it is unclear what the nature of this interaction is.<sup>46</sup> The  $\text{Ca}^{2+}$  ions are unlikely to electrostatically interact with Gs under the experimental conditions, *i.e.* pH  $\sim$  12, since the  $\text{p}K_{\text{A}_{\text{Gs}}} = 10.18$ . Moreover, it has been reported that Gs does not chelate  $\text{Ca}^{2+}$  ions.<sup>47</sup> On the other hand, Cip, which bears a carboxylic acid, is expected to interact with calcium ions by forming a stable complex.<sup>48,49</sup> Therefore, the addition of Cip to the calcium ion solution may enhance its loading into HAP NPs. The addition of the antibiotics to the  $\text{Ca}^{2+}$  solution was followed by the dropwise addition of phosphate, which resulted in the formation of a precipitate that was cleaned and characterized.

Fig. 1 shows TEM images of the Gs-HAP and Cip-HAP powders, which are made of NPs. It is evident that the addition of the antibiotics can affect the morphology of the NPs. Gs-HAP NPs exhibit an elongated shape, whereas the Cip-HAP NPs have a more round morphology. The average size based on TEM was  $20 \pm 8$  nm and  $40 \pm 12$  nm for Gs-HAP and Cip-HAP, respectively. These results are somewhat different from dynamic light scattering (DLS) measurements of diluted dispersions, where the average size for the Gs-HAP and Cip-HAP NPs was  $150 \pm 40$  and  $370 \pm 35$  nm, respectively. This might be related to the high tendency of small NPs to aggregate in the solution. The Cip-HAP aggregates are larger than the Gs-HAP aggregates, which is in accordance with the size of the nanoparticles that form the aggregates.

It can be seen that Gs-HAP NPs are similar to pristine HAP NPs in terms of size and morphology, whereas Cip-HAP NPs have diverse structures. As evidence, the SAED patterns of the drug-loaded HAP NPs powder are shown in Fig. 1S (ESI†). The SAED pattern of pristine HAP shows a typical diffraction of polycrystalline materials, in which visible speckles are seen in the ring. On the other hand, it is hard to distinguish spots in the ring in the SAED patterns of Gs-HAP and Cip-HAP. This implies that the crystal structure of both drug-loaded HAP NPs has lower crystallinity compared with pristine HAP. A comparison between the SAED of Gs-HAP and Cip-HAP shows that Gs-HAP has higher crystallinity. The inner ring of Gs-HAP is characterized by close spots, whereas in the outer ring, the spots are clearly seen. The SAED of Cip-HAP has a more amorphous nature, where there are no visible spots in the ring. SEM images (Fig. 1) are in accordance with the TEM analysis.

The XPS and EDS element analyses (Table 1S, ESI†) were conducted in order to determine the purity of the powder and

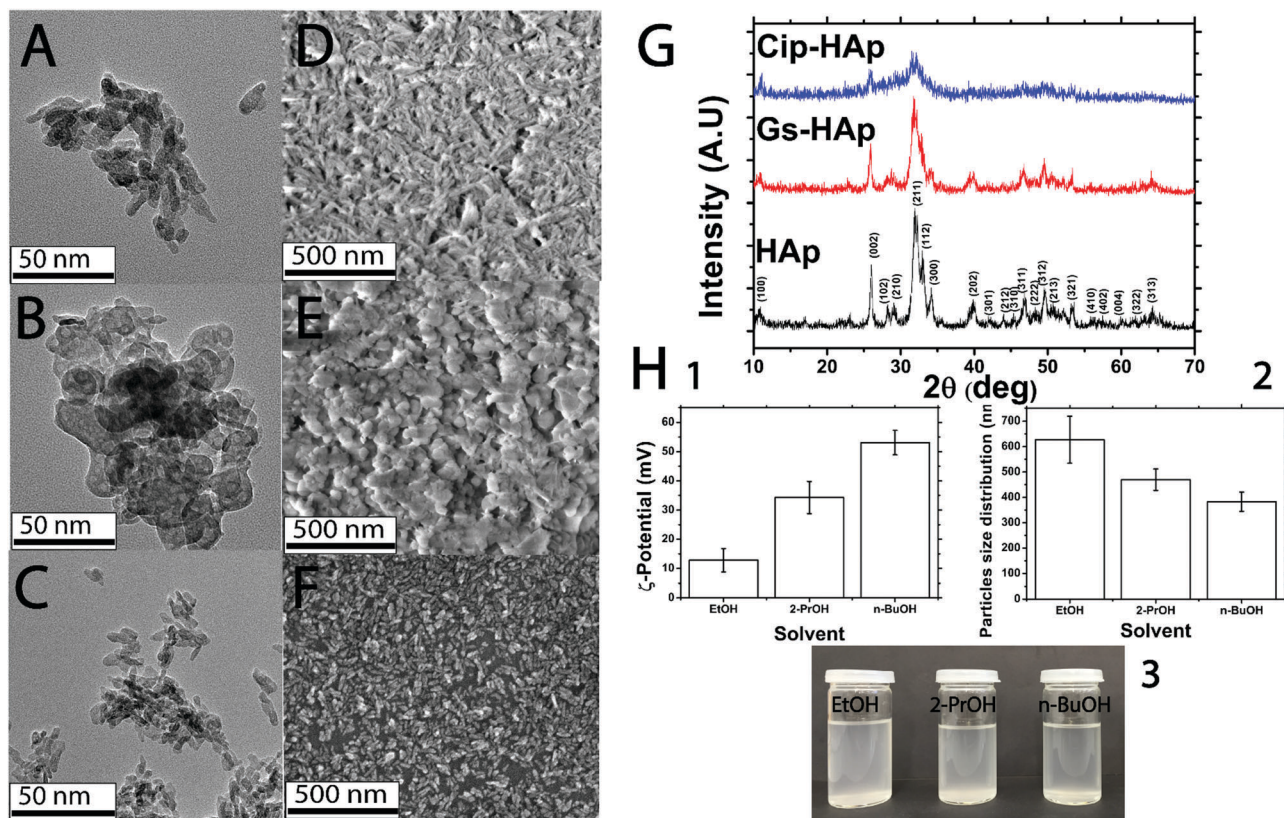


Fig. 1 TEM (A–C) and SEM (D–F) of Gs-HAP, Cip-HAP and HAP, respectively, XRD (G) of pristine and drug-loaded HAP NPs, zeta potential (H.1), particle size distribution (H.2), and digital photo (H.3) of Gs-HAP NP dispersions in different alcoholic solvents.

to verify the encapsulation of the antibiotic into the NPs. The data for the pristine HAP NPs are also shown. The presence of elements such as fluorine and nitrogen can ensure the loading of the drugs. Both EDS and XPS confirm the presence of antibiotics in the HAP NPs. The incorporation of Gs in the HAP NPs is indicated by the presence of N and S, whereas the presence of F and N is attributed to Cip. A detailed discussion appears in Section 3.2.

EDS shows that the atomic Ca/P ratio for both Gs-HAP and Cip-HAP is 1.53, which is somewhat lower than the 1.67 ratio that is expected for HAP. This might imply that the incorporation of the antibiotics into HAP impairs the purity of the phase. On the other hand, it should be noted that EDS analysis is not recommended for unambiguous distinction between different CaP phases.<sup>50</sup> XPS analysis yields a Ca/P ratio of 1.65 and 1.35 for Gs-HAP and Cip-HAP NPs, respectively, which is closer to the expected Ca/P ratio (1.64) for the HAP NPs. On the other hand, the low Ca/P ratio found for the Cip-HAP NPs may imply that the incorporation of Cip during the precipitation of HAP impairs its crystal structure, which is supported also by the SEM and TEM images. At the same time, we conclude that the incorporation of Gs into the HAP NPs did not interfere with the formation of crystalline HAP, where the Ca/P ratio and structure are similar to the HAP NPs. Hence, we speculate that the structure of HAP NPs can be affected depending on the chemical structure of the antibiotic.

XRD measurements were conducted to further verify the phase of the powders and study the impact of antibiotics addition on the crystallinity of the NPs. Fig. 1 shows the XRD patterns of the Gs-HAP and Cip-HAP NPs powders. A comparison between the synthesized HAP and Gs-HAP NPs shows that the incorporation of Gs to HAP does not significantly affect the crystal structure of the lattice. On the other hand, the addition of Cip to the HAP NPs clearly results in a defective crystal structure with substantially lower degree of crystallinity. The calculated degree of crystallinity was 70, 64, and 31% for pristine HAP, Gs-HAP and Cip-HAP, respectively.<sup>51</sup> Thus, these results are in complete agreement with the above XPS, EDS, SEM and TEM findings. The difference in the crystallinity between Gs-HAP and Cip-HAP may be related to the mechanism by which the antibiotics interact with calcium and phosphate ions. Gs is an aminoglycoside antibiotic rich in amine and hydroxyl moieties, and therefore it might interact with the –OH groups of HAP *via* hydrogen bonding or electrostatic interactions. We assume that the hydrogen bonding between the amines and hydroxyl moieties of Gs and the hydroxyl groups of HAP have a minute effect on the crystal structure of HAP. Indeed, it has been reported that the introduction of Gs during HAP precipitation had no effect on its crystalline structure.<sup>52</sup> Cip belongs to the fluoroquinolone family, which is characterized by a fluorine atom bound to the central ring system, and a carboxylic residue. The most reasonable suggestion is that under

Table 1 Weight percentages of the antibiotics in the NPs

	Spectrophotometric (wt%)	Microanalysis (wt%)	XPS (wt%)
Gs-HAP NPs	12.5	10.0	10.5
Cip-HAP NPs	12.8	11.1	12.2

basic conditions, the negatively charged carboxylic groups associate with the calcium ions. Owing to the high concentration of the drug in the solution ( $10 \text{ mg mL}^{-1}$ ), the carboxylic group of Cip is likely to interfere with the precipitation and formation of crystalline HAP.<sup>53</sup> It is important to mention that the exact position of the drugs in the HAP NPs is not fully deduced.

The content of the drugs in the NPs was evaluated by spectrophotometric analysis, XPS and microanalysis (Table 1) in order to determine precisely the wt% of the drug in the NPs. The loading percentage based on XPS and microanalysis measurements was calculated based on the wt% of nitrogen as compared with the theoretical one. Clearly, all the analyses show good agreement. For Gs-HAP, there is a small deviation between the spectrophotometric calculation and both the XPS and microanalysis calculation. This may be a result of the chemical reaction, which is the basis of the spectrophotometric determination, and might increase the error.

It is very probable that the % of loading could have been increased. We have not attempted to optimize it. It depends on the initial concentration and obviously on the interactions between the drugs and the matrix. Yet, what is important is not only the % of loading but the % of release, as will be discussed later.

### 3.2 Drug-loaded HAP dispersions

Low-molecular weight alcohols, such as methanol, ethanol, 2-propanol, and *n*-butanol, have been the most common solvents for the EPD of HAP NPs.<sup>54,55</sup> TEOA has been reported as an efficient dispersant; therefore, it had been added in order to increase the stability of the dispersions and the electrophoretic mobility of the particles.<sup>56</sup> Firstly, we tried to obtain stable dispersions of the NPs in ethanol, 2-propanol, and *n*-butanol. The  $\zeta$ -potential and particle size distribution of Gs-HAP show that *n*-butanol is the optimal solvent for dispersing these NPs (Fig. 1). Clearly, the NPs possess positive charge in these solvents. The maximum concentration of Gs-HAP NPs, where a stable dispersion is still maintained, was 0.5% w/w. Based on similar experiments, 2-propanol was selected for dispersing Cip-HAP NPs without TEOA addition. The maximum concentration of Cip-HAP in the dispersion without further sedimentation was 0.25% w/w.

### 3.3 EPD and coating characterization

After stabilizing the drug-loaded NPs in an organic solvent, we studied their EPD on Ti surfaces. Fig. 2 shows SEM images (at different magnifications) of the Gs-HAP and Cip-HAP NP coatings. It can be seen that in both cases homogeneous coatings in terms of morphology and composition are obtained. Yet, there are some differences between the two layers.

Specifically, the Cip-HAP NP coating has less cracks and is less rough than Gs-HAP (Table 2). The difference is attributed to the thickness of the coating. We found that applying the same conditions (*i.e.* potential and time) resulted in substantially thicker films of Cip-HA NPs. Yet, the adhesion of the Cip-HAP NPs to the titanium was significantly worse than that of the Gs-NPs (Table 2). Therefore, we had to apply less negative potentials for the EPD of Cip-HAP, which yielded a  $9.3 \text{ }\mu\text{m}$ -thick coating after 5 min, compared with a  $24.7 \text{ }\mu\text{m}$ -thick Gs-HAP NP coating after the same deposition time. Hence, we attribute the cracks formed in the Gs-HAP coating to its greater thickness. As the coating becomes thicker, its tendency to form cracks is higher due to mechanical stresses related to shrinkage of the coating during drying.<sup>54</sup>

These results indicate that the EPD is strongly affected by the drugs loaded into the HAP NPs. This is most likely due to the effect of the adsorbed drug on the  $\zeta$ -potential, which clearly affects the rate of deposition. It is also probable that the lower crystallinity of Cip-HAP NPs influences the adhesion; however, we have no proof for this.

XPS analysis of the coatings was conducted in order to ensure the presence of drug (Table 2S, ESI<sup>†</sup>). The detection of fluorine as well as nitrogen unambiguously indicates that each coating contains its relevant antibiotics. A comparison between the XPS analyses of drug-loaded HAP NPs before and after EPD (Table 1S, ESI<sup>†</sup>) shows that the element ratios in the coatings are similar, indicating that the drugs were not eluted during the EPD process. The total antibiotic amount in the coating was calculated by dissolving the coatings with HCl (0.5 M) and determining the released drugs by spectrophotometry. The total amount of Gs and Cip in the coatings was  $360 \pm 13$  and  $101 \pm 8 \text{ }\mu\text{g cm}^{-2}$ , respectively. Recalling that the mass of the coating was 7.7 and 2.1 mg for Gs-HAP and Cip-HAP, respectively (Table 1), and taking into account the area that was coated ( $2.68 \text{ cm}^2$ ), we get that the wt% of Gs and Cip is 12.5% and 12.9%, respectively. These values are similar to the wt% reported above (namely, 12.5% and 12.8%, respectively) for the NPs before coating. The total drug loading calculation by XPS reveals similar percentages compared with the NPs, *i.e.* 9.5% and 13.2% for Gs-HAP and Cip-HAP coatings, respectively.

Fig. 2 shows the XRD patterns of Gs-HAP and Cip-HAP coatings on titanium. The four intense peaks are related to the titanium substrate (ICSD-PDF2 file 04-002-2539). While the pattern of the Gs-HAP deposit shows the characteristic peaks of HAP, the HAP reflections in the Cip-HAP coating are barely observed. Poor crystallinity of Cip-HAP NPs and low thickness of the deposit are the main reasons of this. Moreover, the calculation for HAP-Cip shows a small average crystallite size of *ca.*  $63.1 \text{ }\text{\AA}$ , whereas the average crystallite size of HAP-Gs was  $129.2 \text{ }\text{\AA}$ . The small crystallite size may also contribute to the broadened spectrum according to the Scherrer equation.<sup>57</sup>

The FTIR spectrum (Fig. 2) shows the typical HAP peaks:  $\text{PO}_4^{3-}$  vibration peaks at 565, 607, 962, 1026, 1078, and  $1146 \text{ cm}^{-1}$ .<sup>58,59</sup> In addition,  $\text{OH}^-$  vibrations are observed at 630 and  $3540 \text{ cm}^{-1}$ . The spectrum of Cip-HAP exhibits different patterns. The peak at  $1272 \text{ cm}^{-1}$  is attributed to the C-F vibration of Cip. The peak at

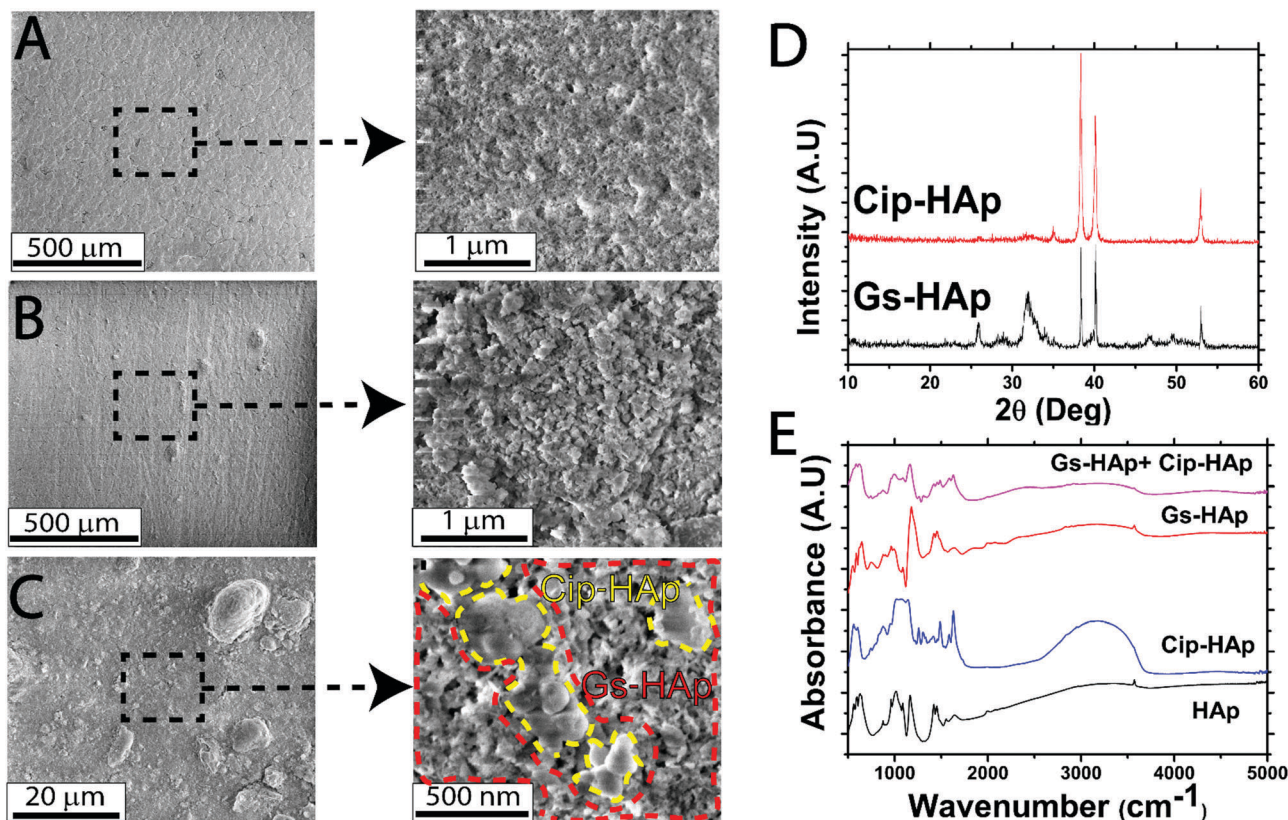


Fig. 2 SEM (A–C) images at different magnifications of Gs-HAp, Cip-HAp, and Gs-HAp + Cip-HAp NPs coatings, respectively. The dashed yellow lines emphasize the co-deposition of Cip-HAp and Gs-HAp. XRD (D) of drug-loaded HAp NP coatings, and FTIR spectrum (E) of drug-loaded HAp NPs.

Table 2 Summary of selected properties of the two coatings

	Thickness (μm)	Roughness (μm)	Adhesion (MPa)	Deposit weight (mg)
Gs-Hap	24.7 ± 0.3	2.31 ± 0.26	5.8 ± 0.7	7.7 ± 0.6
Cip-Hap	9.3 ± 1.3	0.37 ± 0.07	13.7 ± 2.1	2.1 ± 0.1

1627  $\text{cm}^{-1}$  is attributed to carbonyl  $\text{C}=\text{O}$  stretching vibrations. The peaks at 1584 and 1384  $\text{cm}^{-1}$  are assigned to stretching vibrations of  $\text{COO}^-$ .<sup>60–62</sup> The small peaks at 1546 and 1638  $\text{cm}^{-1}$  in the Gs-HAp spectrum may be associated with bending vibration of primary amines, and the peaks between 2850 and 3000 are related to  $\text{CH}_2$ - stretching vibrations.<sup>63,64</sup> In addition, in both spectra (Gs and Cip-HAp), the characteristics peaks of HAp are highly masked by the incorporation of the antibiotics by hydrogen bonding to P-OH groups. The spectrum of the mixed coating shows the incorporation of Cip. On the other hand, the determination of Gs in the coating is not conclusive.

One of the advantages of using pre-drug-loaded HAp NPs is the possibility of incorporating several types of antibiotics followed by their deposition in a single step. The integration of a couple of drugs, such as Gs and Cip, can critically reduce the risk of implant infections due to the wider spectrum of antibacterial activity. In our research, we managed to disperse both Gs-HAp and Cip-HAp in the same solution and deposit them simultaneously to produce a drug-loaded coating with

improved antimicrobial spectrum. Fig. 2 shows the drug-loaded coating composed of Gs-HAp and Cip-HAp. It can be seen that the coating is composed of both Gs-HAp and Cip-HAp NPs, as the former has elongated morphology whereas the latter is characterized by rounded morphology. XPS element analysis (Table 3S, ESI<sup>†</sup>) was conducted to assure the presence of both drugs. As mentioned before, the presence of F and N in the coating can verify that indeed the deposition of both drug-loaded HAp NPs was accomplished.

Spectrophotometric determination of the loading amounts of each drug in the coating has significant limitation due to similar functional groups, such as primary and secondary amines. Hence, the calculation of each drug was based on XPS analysis. Cip was determined by the F wt%, whereas Gs by the N wt% after reducing the relative percent related to Cip. The calculated wt% of Cip and Gs in the mixed coating was ca. 8% and 4.4%, respectively.

### 3.4 Drug-release studies

Fig. 3 shows the kinetics of release of the antibiotics *in vitro*, *i.e.*, the total drug amount released and the cumulative release percentage as a function of time per measurement. The data are average of triplicates. The detection limit for Gs and Cip was 4.97 and 0.13  $\mu\text{g mL}^{-1}$ , respectively. An initial burst in the first day can be seen in both the profiles, which is followed by a slow release. For the Cip-HAp coating, the release of the drug ceases

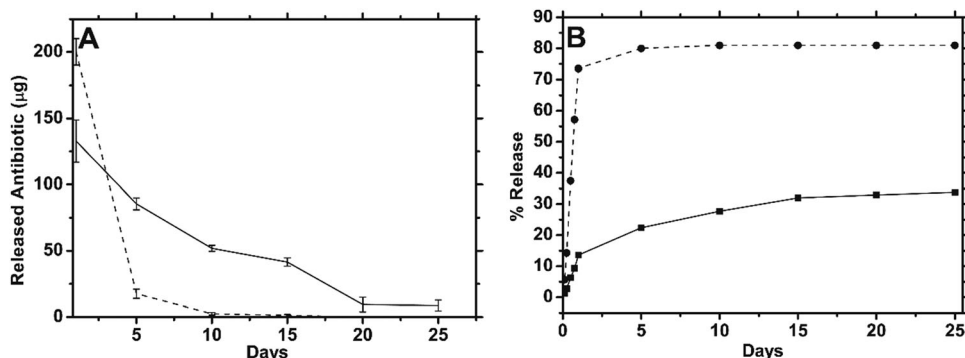


Fig. 3 Release profile of Gs-HAP (solid) and Cip-HAP (dashed). (A) Total drug amount, (B) cumulative release percentage.

after 10 day, as *ca.* 80% of the deposited drug is eluted to the aqueous solution. In contrast, Gs is continuously eluted from the coating for 25 days. However, only *ca.* 30% of the total loaded drug is released. This might be attributed to the thickness of the coating. The latter is smaller for Cip-HAP as compared with the Gs-HAP coating, which results in greater penetration of water into the coating and increase in drug dissolution. The thicker coating for Gs-HAP presumably affects also the total lower percentage of drug that is released. Yet, the remaining drug inside the coating may be eluted *in vivo* during the regeneration of ingrowing bone tissue towards the implant.

In order to assess the effect of the coating on the release, we examined also the release of the drugs from the antibiotic-loaded HAP NPs dispersed in the same buffer as above. Specifically, 10 mg of Gs-HAP and Cip-HAP NPs were stirred in PBS at pH 7.4. After 2 hours, the solution was centrifuged, and 1 mL of the supernatant was analyzed spectrophotometrically. We found that approximately 94% of the drug was released during the first two hours. After 4 hours, the rest of the drug was eluted. This clearly shows that the difference between the release profiles of the Gs-HAP NP and Cip-HAP NP coatings is likely to be related to the morphology and structure of the deposit; thicker layers attain slower release of the encapsulated drug as compared with thin coatings.

The SEM images (Fig. 2S, ESI†) of the drug-loaded HAP NP coatings before and after 25 days of immersion in PBS reveal interesting implications regarding the encapsulation of the drugs inside the NPs. It can be seen that the morphology of both Gs-HAP and Cip-HAP was changed. For both coatings, the size of the deposited NPs shrank, especially for Cip-HAP, for which the structure of the coating was significantly modified. The round structure of Cip-HAP was transformed into needle-like particles. These results may imply that indeed the drugs were encapsulated into the HAP NPs, and as a result of water penetration the drugs were dissolved into the aqueous media, which resulted in the particles shirking.

### 3.5 *In vitro* bioactivity test

The tendency of a coated substrate to stimulate bone regeneration plays a significant role in the implantation success.<sup>40</sup> HAP as the main component of human bone promotes bone formation by adsorbing minerals from the body fluids and enhances the

biomineralization of the coated implant.<sup>18,39,40</sup> The bioactivity test was conducted on a commercial dental titanium implant. Fig. 4 shows the SEM images of a titanium implant coated with Gs-HAP before immersion in SBF for 4 weeks. Clearly, the nanoparticulate coating is deposited very homogeneously on the titanium implant, thus showing that complex geometries of the substrate do not affect the morphology of the coating. Fig. 4 shows the SEM images of the coated substrate after 4 weeks of immersion in SBF at  $37 \pm 1$  °C. The bioactive nature of the coated titanium shows a significant adsorbing property. The precipitation of apatite crystals on the coated materials may resemble the biomineralization *in vivo*. It has been reported that the formation of an apatite layer *in vitro* by HAP suggests its ability to strongly interact with living bone *in vivo*.<sup>65</sup> Fig. 3S (ESI†) shows SEM images of a Gs-HAP coated titanium implant and an uncoated titanium implant after 4 weeks if immersion in SBF solution. Clearly, biomineralization of the implant occurred only in the coated implant indicating, the bioactive nature of the drug-loaded coating. On the other hand, the morphology of the uncoated implant remained the same, without any indication of precipitation of inorganic materials.

Further insight on the biomineralization of the Gs-HAP coating was gained from the EDS element analysis given in Table 1S (ESI†). It is evident that the layer that grew on the coated implant is primarily made of apatite, but contains also a low percentage of other minerals.<sup>18</sup> The presence of ions such as  $\text{Na}^+$ ,  $\text{Mg}^{+2}$ , and  $\text{Cl}^-$  clearly indicates the biomineralization of the implant *in vitro*. The precipitation of these ions from the SBF solution towards the implant is attributed to the positive ( $\text{Ca}^{+2}$ ) and the negative ( $\text{PO}_4^{-3}$  and  $\text{OH}^-$ ) sites on the HAP coating. The spontaneous formation of an apatite layer on the HAP NP-based coating containing antibiotics suggests that the presence of the drug did not interfere with the formation of a new apatite layer. Thus, the combination between HAP and antibiotics such as Gs and Cip can guarantee superior osteoconductivity combined with antibacterial properties. This unique synergy has a crucial role in determining the success of implantation by simultaneously promoting bone formation and reducing the risk of infections.

### 3.6 Antibacterial activity

Evaluation of the antibacterial activity of the drug-loaded HAP NP coatings is crucial due to the fact that non-trivial conditions

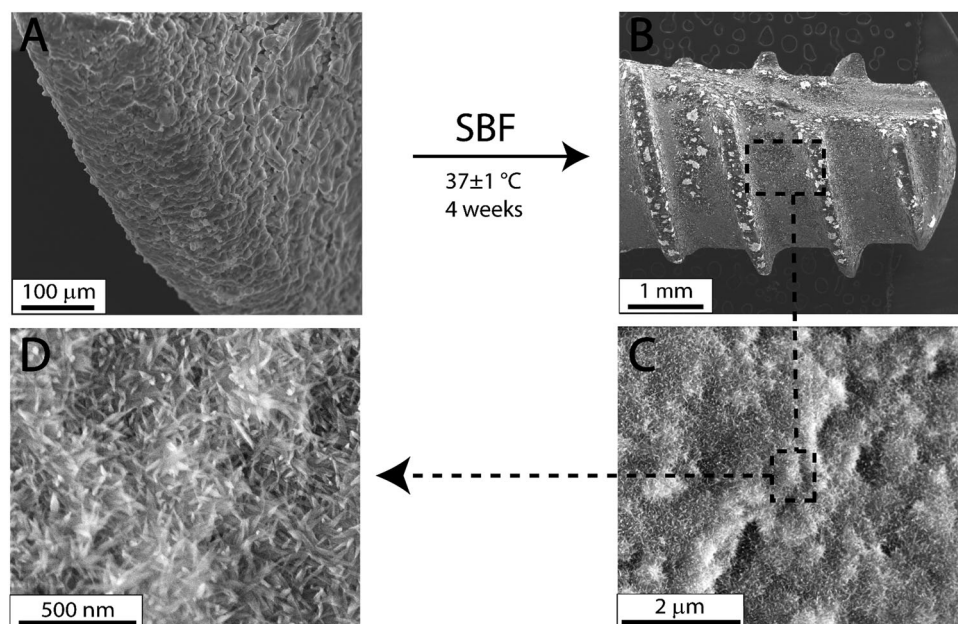


Fig. 4 SEM images of a dental implant coated with Gs-HAp NPs; (A) before and (B–D) after 4 weeks of immersion in SBF at  $37 \pm 1$  °C.

(high pH, 1 h at boiling point and high voltage) were used in order to synthesize and deposit the drug-loaded HAP NPs. The antibacterial activity was performed against *P. aeruginosa*, a common bacteria, which is associated with bone infections.<sup>2</sup> Cip and Gs are well-known antibiotics that have efficient antimicrobial activity against Gram-negative bacteria such as *P. aeruginosa*. The drug-loaded HAP NP coatings were scraped from the titanium substrates and dispersed in PBS solution under sonication in order to release the antibiotics from the NPs. After centrifugation, the supernatants were tested against the *P. aeruginosa* bacteria. Pristine HAP NP coatings were used

as a negative control in order to show that neither HAP nor PBS has any antimicrobial activity. Pure Gs and Cip solutions ( $100 \text{ mg mL}^{-1}$  in PBS) were used as a positive control. Fig. 5 shows that the drug-loaded HAP NPs have efficient antibacterial activity compared with the positive control. These results confirmed that both the synthesis and the EPD do not impair the antibacterial properties of Cip and Gs. The average inhibition diameters of Cip and Gs-HAP NPs were  $2.11 \pm 0.07$ ,  $2.53 \pm 0.05$  cm, respectively. These results were similar to the positive control  $2.26 \pm 0.08$  and  $2.73 \pm 0.1$  cm for Gs and Cip solution, respectively. Hence, the performance of Gs and Cip is not impaired by the synthesis and

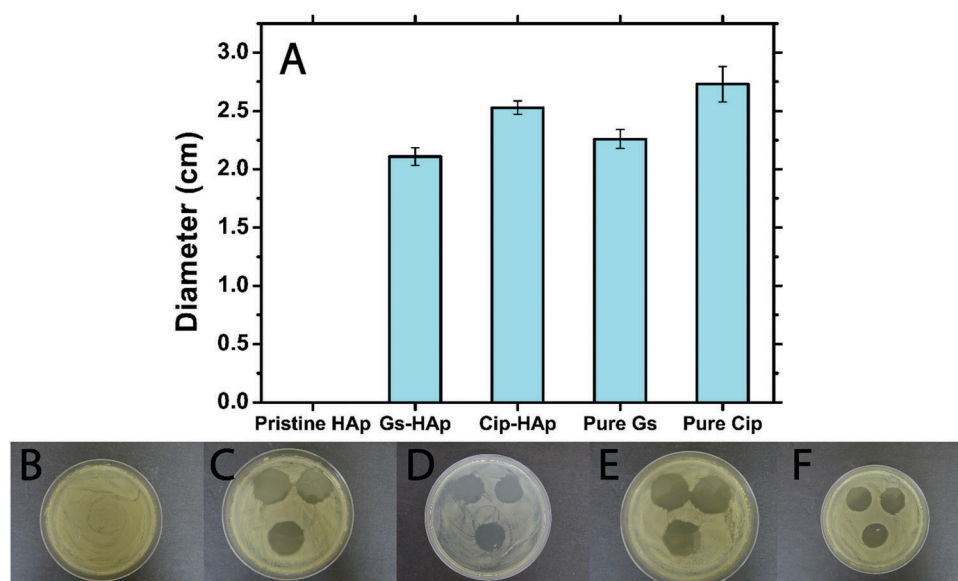


Fig. 5 Summary of agar diffusion tests performed with *P. aeruginosa* bacteria. (A) Average and standard deviation of inhibition diameters of different diffusion tests. (B–F) Images of agar diffusion test of pristine HAp, Cip-HAp, Gs-HAp, pure Cip and pure Gs, respectively.

EPD conditions, and therefore the antibiotics can be well-combined with the HAp NPs to produce biocompatible coatings with excellent antibacterial activity.

## 4. Conclusions

The drug-loaded HAp NPs were synthesized by a wet chemical reaction, where Gs or Cip was introduced during the formation of the HAp NPs. The loading percent of Gs and Cip determined spectrophotometrically was *ca.* 12.5% and 12.8%, respectively. XPS, XRD, and EDS confirmed the encapsulation of Gs and Cip in the HAp NPs. Electrophoretic deposition was used for the first time to coat titanium dental implants with the drug-loaded HAp nanoparticles in a single, simple step. This approach yielded a pure HAp coating with antibiotics without any additional additives. Moreover, a wider-spectrum antibacterial coating was obtained by depositing both Gs- and Cip-HAp simultaneously. The coated implants showed release of Gs and Cip for up to 25 (25% release) and 10 (>95% release) days, respectively, where 70% of the encapsulated Cip was released within the first 24 hours. The osteoconductivity of the method was tested by using a commercial titanium dental implant. The coated implant showed high bioactivity by enhancing the precipitation of ions from the SBF solution, which resembles the *in vitro* biomineralization of the implant. *In vitro* antibacterial tests proved that the synthesis and deposition conditions did not deteriorate the antimicrobial activity of the drug-loaded HAp NPs. Both Gs and Cip-HAp NP coatings exhibited high efficiency in inhibiting the growth of *P. aeruginosa* bacteria.

Our approach that is based on two major elements, the use of nanoparticles as drug carriers and the formation of a film by depositing nanomaterials, has several significant advantages. Firstly, it enables complex geometries to be coated with HAp and various drugs in a single step. Secondly, since the deposition is carried out at room temperature, the process is harmless to the drugs. Finally, the nanoparticulate character of the coating makes it a superior platform for controlling very well the release of the drug also from inside the coating, and at the same time has an excellent osteoconductivity effect, presumably due to the high surface area. We believe that this approach could be further explored for other implants, drugs, and coatings.

## Conflicts of interest

There are no conflicts to declare.

## Acknowledgements

This study was financially supported by a Kamin grant 52694-5 from the Israel Ministry of Economy. The partial support by the Focal Technology Area through the Israel National Nanotechnology Initiative (INNI) is acknowledged. The Harvey M. Krueger Family Centre for Nanoscience and Nanotechnology of the Hebrew University is acknowledged. We thank SGS Dental for providing us with commercial dental implants to test our coatings.

## References

- 1 M. E. Hake, H. Young, D. J. Hak, P. F. Stahel, E. M. Hammerberg and C. Mauffrey, Local antibiotic therapy strategies in orthopaedic trauma: Practical tips and tricks and review of the literature, *Injury*, 2015, **46**, 1447–1456.
- 2 D. P. Lew and F. A. Waldvogel, Osteomyelitis, *J.-Lancet*, 2004, **364**, 369–379.
- 3 N. Eliaz and N. Metoki, Calcium Phosphate Bioceramics: A Review of Their History, Structure, Properties, Coating Technologies and Biomedical Applications, *Materials*, 2017, **10**, 334.
- 4 H. Alvarez, C. Castro, L. Moujir, A. Perera, A. Delgado and I. Soriano, *et al.*, Efficacy of ciprofloxacin implants in treating experimental osteomyelitis, *J. Biomed. Mater. Res., Part B*, 2008, **85**, 93–104.
- 5 S. R. Bhalerao and A. R. Rote, Application of UV spectrophotometric methods for estimation of ciprofloxacin and tinidazole in combined tablet dosage form, *Int. J. Pharm. Pharm. Sci.*, 2012, **4**, 464–467.
- 6 M. Zilberman and J. J. Elsner, Antibiotic-eluting medical devices for various applications, *J. Controlled Release*, 2008, **130**, 202–215.
- 7 P. J. Carek, L. M. Dickerson and J. L. Sack, Diagnosis and management of osteomyelitis, *Am. Fam. Physician*, 2001, **63**, 2413–2420.
- 8 G. Cierny Iii, J. T. Mader and J. J. Penninck, The Classic: A Clinical Staging System for Adult Osteomyelitis, *Clin. Orthop. Relat. Res.*, 2003, **414**, 7–24.
- 9 R. S. Edson and C. L. Terrell, *The aminoglycosides*, Mayo Clinic Proceedings, Elsevier, 1999, pp. 519–528.
- 10 H. Wahlig, E. Dingeldein, R. Bergmann and K. Reuss, The release of gentamicin from polymethylmethacrylate beads. An experimental and pharmacokinetic study, *J. Bone Jt. Surg.*, 1978, **60**, 270–275.
- 11 J. S. Gogia, J. P. Meehan, P. E. Di Cesare and A. A. Jamali, *Local antibiotic therapy in osteomyelitis. Seminars in plastic surgery*, © Thieme Medical Publishers, 2009, pp. 100–107.
- 12 S. K. Nandi, P. Mukherjee, S. Roy, B. Kundu, D. K. De and D. Basu, Local antibiotic delivery systems for the treatment of osteomyelitis—A review, *Mater. Sci. Eng., C*, 2009, **29**, 2478–2485.
- 13 S. M. Abdelghany, D. J. Quinn, R. J. Ingram, B. F. Gilmore, R. F. Donnelly and C. C. Taggart, *et al.*, Gentamicin-loaded nanoparticles show improved antimicrobial effects towards *Pseudomonas aeruginosa* infection, *Int. J. Nanomed.*, 2012, **7**, 4053–4063.
- 14 Y.-C. Huang and R.-Y. Li, Preparation and characterization of antioxidant nanoparticles composed of chitosan and fucoidan for antibiotics delivery, *Mar. Drugs*, 2014, **12**, 4379–4398.
- 15 V. Mouriño and A. R. Boccaccini, Bone tissue engineering therapeutics: controlled drug delivery in three-dimensional scaffolds, *J. R. Soc., Interface*, 2010, **7**, 209–227.
- 16 J. A. Jansen and B. Leon, *Thin calcium phosphate coatings for medical implants*, Springer, 2009.

- 17 R. Z. LeGeros, Calcium phosphates in oral biology and medicine, *Monogr. Oral Sci.*, 1990, **15**, 1–201.
- 18 R. Murugan and S. Ramakrishna, Development of nano-composites for bone grafting, *Compos. Sci. Technol.*, 2005, **65**, 2385–2406.
- 19 B. D. Ratner, A. S. Hoffman, F. J. Schoen and J. E. Lemons, *Biomaterials science: an introduction to materials in medicine*, Academic Press, 2004.
- 20 T. J. Webster, Nanophase ceramics: the future orthopedic and dental implant material, *Adv. Chem. Eng.*, 2001, **27**, 125–166.
- 21 F. Hilbrig and R. Freitag, *Hydroxyapatite in bioprocessing. Biopharmaceutical Production Technology*, 2012, vol. 1–2, pp. 283–331.
- 22 M. Mittal, S. Nath and S. Prakash, Improvement in mechanical properties of plasma sprayed hydroxyapatite coatings by Al<sub>2</sub>O<sub>3</sub> reinforcement, *Mater. Sci. Eng., C*, 2013, **33**, 2838–2845.
- 23 R. Asri, W. Harun, M. Hassan, S. Ghani and Z. Buyong, A review of hydroxyapatite-based coating techniques: Sol-gel and electrochemical depositions on biocompatible metals, *J. Mech. Behav. Biomed. Mater.*, 2016, **57**, 95–108.
- 24 B. Mavis and A. C. Taş, Dip Coating of Calcium Hydroxyapatite on Ti–6Al–4V Substrates, *J. Am. Ceram. Soc.*, 2000, **83**, 989–991.
- 25 O. Geuli, N. Metoki, N. Eliaz and D. Mandler, Electrochemically Driven Hydroxyapatite Nanoparticles Coating of Medical Implants, *Adv. Funct. Mater.*, 2016, **26**, 8003–8010.
- 26 R. Bosco, M. Iafisco, A. Tampieri, J. A. Jansen, S. C. Leeuwenburgh and J. J. Van Den Beucken, Hydroxyapatite nanocrystals functionalized with alendronate as bioactive components for bone implant coatings to decrease osteoclastic activity, *Appl. Surf. Sci.*, 2015, **328**, 516–524.
- 27 N. Eliaz, T. M. Sridhar, U. K. Mudali and B. Raj, Electrochemical and electrophoretic deposition of hydroxyapatite for orthopaedic applications, *Surf. Eng.*, 2005, **21**, 238–242.
- 28 B. Tian, S. Tang, C.-D. Wang, W.-G. Wang, C.-L. Wu and Y.-J. Guo, *et al.*, Bactericidal properties and biocompatibility of a gentamicin-loaded Fe<sub>3</sub>O<sub>4</sub>/carbonated hydroxyapatite coating, *Colloids Surf., B*, 2014, **123**, 403–412.
- 29 F. Laurent, A. Bignon, J. Goldnadel, J. Chevalier, G. Fantozzi and E. Viguier, *et al.*, A new concept of gentamicin loaded HAP/TCP bone substitute for prophylactic action: *in vitro* release validation, *J. Mater. Sci.: Mater. Med.*, 2008, **19**, 947–951.
- 30 F. Pishbin, V. Mouriño, S. Flor, S. Kreppel, V. Salih and M. P. Ryan, *et al.*, Electrophoretic deposition of gentamicin-loaded bioactive glass/chitosan composite coatings for orthopaedic implants, *ACS Appl. Mater. Interfaces*, 2014, **6**, 8796–8806.
- 31 J. Zhang, Z. Wen, M. Zhao, G. Li and C. Dai, Effect of the addition CNTs on performance of CaP/chitosan/coating deposited on magnesium alloy by electrophoretic deposition, *Mater. Sci. Eng., C*, 2016, **58**, 992–1000.
- 32 W. H. Traub and B. Leonhard, Heat stability of the antimicrobial activity of sixty-two antibacterial agents, *J. Antimicrob. Chemother.*, 1995, **35**, 149–154.
- 33 S. Gummadi, D. Thota, S. V. Varri, P. Vaddi and V. L. N. S. Rao, Development and validation of UV spectroscopic methods for simultaneous estimation of ciprofloxacin and tinidazole in tablet formulation, *Int. Curr. Pharm. J.*, 2012, **1**, 317–321.
- 34 S. S. Sampath and D. H. Robinson, Comparison of new and existing spectrophotometric methods for the analysis of tobramycin and other aminoglycosides, *J. Pharm. Sci.*, 1990, **79**, 428–431.
- 35 P. F. Cabanillas, E. De Peña, J. Barrales-Rienda and G. Frutos, Validation and *in vitro* characterization of antibiotic-loaded bone cement release, *Int. J. Pharm.*, 2000, **209**, 15–26.
- 36 I. H. T. Guideline, *Validation of analytical procedures: text and methodology*, 2005, **Q2(R1)**, 1.
- 37 N. Eliaz, O. Ritman-Hertz, D. Aronov, E. Weinberg, Y. Shenhar and G. Rosenman, *et al.*, The effect of surface treatments on the adhesion of electrochemically deposited hydroxyapatite coating to titanium and on its interaction with cells and bacteria, *J. Mater. Sci.: Mater. Med.*, 2011, **22**, 1741–1752.
- 38 A. Standard, *C633-01 (2008) Standard Test Method for Adhesion or Cohesion Strength of Thermal Spray Coatings*, ASTM International, West Conshohocken, PA, 2008.
- 39 P. N. Chavan, M. M. Bahir, R. U. Mene, M. P. Mahabole and R. S. Khairnar, Study of nanobiomaterial hydroxyapatite in simulated body fluid: Formation and growth of apatite, *Mater. Sci. Eng., B*, 2010, **168**, 224–230.
- 40 T. Kokubo and H. Takadama, How useful is SBF in predicting *in vivo* bone bioactivity?, *Biomaterials*, 2006, **27**, 2907–2915.
- 41 M. Wei, A. Ruys, B. Milthorpe and C. Sorrell, Precipitation of hydroxyapatite nanoparticles: effects of precipitation method on electrophoretic deposition, *J. Mater. Sci.: Mater. Med.*, 2005, **16**, 319–324.
- 42 M. Wei, A. Ruys, B. Milthorpe, C. Sorrell and J. Evans, Electrophoretic deposition of hydroxyapatite coatings on metal substrates: a nanoparticulate dual-coating approach, *J. Sol-Gel Sci. Technol.*, 2001, **21**, 39–48.
- 43 G. D. Georgiev, G. A. Georgiev and Z. Lalchev, Interaction of gentamicin with phosphatidylserine/phosphatidylcholine mixtures in adsorption monolayers and thin liquid films: morphology and thermodynamic properties, *Eur. Biophys. J.*, 2010, **39**, 1301–1312.
- 44 H. D. Humes, M. Sastrasinh and J. Weinberg, Calcium is a competitive inhibitor of gentamicin-renal membrane binding interactions and dietary calcium supplementation protects against gentamicin nephrotoxicity, *J. Clin. Invest.*, 1984, **73**, 134.
- 45 A. B. Coffin, K. E. Reinhart, K. N. Owens, D. W. Raible and E. W. Rubel, Extracellular divalent cations modulate aminoglycoside-induced hair cell death in the zebrafish lateral line, *Hear. Res.*, 2009, **253**, 42–51.
- 46 V. M. Tiwow, Determination of stability constants of aminoglycoside antibiotics with their metal complexes, 4th International Conference On Mathematics And Natural Sciences (ICMNS 2012): Science for Health, Food and Sustainable Energy, AIP Publishing, 2014, pp. 426–430.
- 47 S. J. Kohlhepp, S. B. Plant, D. A. McCarron and D. N. Gilbert, Gentamicin does not chelate calcium, *Antimicrob. Agents Chemother.*, 1982, **21**, 668–669.

- 48 A. Stojković, L. Tajber, K. J. Paluch, Z. Djurić, J. Parojčić and O. I. Corrigan, Biopharmaceutical characterisation of ciprofloxacin-metallic ion interactions: Comparative study into the effect of aluminium, calcium, zinc and iron on drug solubility and dissolution, *Acta Pharm.*, 2014, **64**, 77–88.
- 49 S. Upadhyay, P. Kumar and V. Arora, Complexes of quinolone drugs norfloxacin and ciprofloxacin with alkaline earth metal perchlorates, *J. Struct. Chem.*, 2006, **47**, 1078–1083.
- 50 M. J. Bailey, S. Coe, D. M. Grant, G. W. Grime and C. Jeynes, Accurate determination of the Ca:P ratio in rough hydroxyapatite samples by SEM-EDS, PIXE and RBS – a comparative study, *X-Ray Spectrom.*, 2009, **38**, 343–347.
- 51 E. Landi, A. Tampieri, G. Celotti and S. Sprio, Densification behaviour and mechanisms of synthetic hydroxyapatites, *J. Eur. Ceram. Soc.*, 2000, **20**, 2377–2387.
- 52 D. Tadic, T. Welzel, P. Seidel, E. Wüst, E. Dingeldein and M. Epple, Controlled release of gentamicin from biomimetic calcium phosphate *in vitro*. Comparison of four different incorporation methods, *Materialwiss. Werkstofftech.*, 2004, **35**, 1001–1005.
- 53 H. Bouyarmane, I. El Hanbali, M. El Karbane, A. Rami, A. Saoiabi and S. Saoiabi, *et al.*, Parameters influencing ciprofloxacin, ofloxacin, amoxicillin and sulfamethoxazole retention by natural and converted calcium phosphates, *J. Hazard. Mater.*, 2015, **291**, 38–44.
- 54 M. Farrokhi-Rad and T. Shahrabi, Effect of suspension medium on the electrophoretic deposition of hydroxyapatite nanoparticles and properties of obtained coatings, *Ceram. Int.*, 2014, **40**, 3031–3039.
- 55 X. F. Xiao and R. F. Liu, Effect of suspension stability on electrophoretic deposition of hydroxyapatite coatings, *Mater. Lett.*, 2006, **60**, 2627–2632.
- 56 M. Farrokhi-Rad and T. Shahrabi, Effect of triethanolamine on the electrophoretic deposition of hydroxyapatite nanoparticles in isopropanol, *Ceram. Int.*, 2013, **39**, 7007–7013.
- 57 X. Zhu, O. Eibl, L. Scheideler and J. Geis-Gerstorfer, Characterization of nano hydroxyapatite/collagen surfaces and cellular behaviors, *J. Biomed. Mater. Res., Part A*, 2006, **79**, 114–127.
- 58 M. Corno, C. Busco, B. Civalleri and P. Ugliengo, Periodic ab initio study of structural and vibrational features of hexagonal hydroxyapatite  $\text{Ca}_{10}(\text{PO}_4)_6(\text{OH})_2$ , *Phys. Chem. Chem. Phys.*, 2006, **8**, 2464–2472.
- 59 L. Berzina-Cimdina and N. Borodajenko, *Research of calcium phosphates using Fourier transform infrared spectroscopy*, INTECH Open Access Publisher, 2012.
- 60 S. Sahoo, C. K. Chakraborti, S. C. Mishra, U. Nanda and S. Naik, *FTIR and XRD investigations of some fluoroquinolones*, 2011.
- 61 S. Agnihotri, R. Pathak, D. Jha, I. Roy, H. K. Gautam and A. K. Sharma, *et al.*, Synthesis and antimicrobial activity of aminoglycoside-conjugated silica nanoparticles against clinical and resistant bacteria, *New J. Chem.*, 2015, **39**, 6746–6755.
- 62 G. S. Kumar, R. Govindan and E. K. Girija, *In situ* synthesis, characterization and *in vitro* studies of ciprofloxacin loaded hydroxyapatite nanoparticles for the treatment of osteomyelitis, *J. Mater. Chem. B*, 2014, **2**, 5052–5060.
- 63 H. Pandey, V. Parashar, R. Parashar, R. Prakash, P. W. Ramteke and A. C. Pandey, Controlled drug release characteristics and enhanced antibacterial effect of graphene nanosheets containing gentamicin sulfate, *Nanoscale*, 2011, **3**, 4104–4108.
- 64 C. McManamon, J. P. de Silva, P. Delaney, M. A. Morris and G. L. Cross, Characteristics, interactions and coating adherence of heterogeneous polymer/drug coatings for biomedical devices, *Mater. Sci. Eng., C*, 2016, **59**, 102–108.
- 65 M. Neo, S. Kotani, T. Nakamura, T. Yamamuro, C. Ohtsuki and T. Kokubo, *et al.*, A comparative study of ultrastructures of the interfaces between four kinds of surface-active ceramic and bone, *J. Biomed. Mater. Res.*, 1992, **26**, 1419–1432.